Pressure-dependent spin fluctuations and magnetic structure in the topologically frustrated spin glass alloy $Y(Mn_{0.95}Al_{0.05})_2$

M. T. F. Telling,[1,2,*] K. S. Knight,[1] F. L. Pratt,[1] A. J. Church,[1] P. P. Deen,[3,4] K. J. Ellis,[5] I. Watanabe,[6] and R. Cywinski[5]

[1]*ISIS Facility, Rutherford Appleton Laboratory, Chilton, OX11 0QX, United Kingdom*

[2]*Department of Materials, University of Oxford, Parks Road, Oxford, OX1 3PH, United Kingdom*

[3]*Institut Laue-Langevin, BP 156, 6, rue Jules Horowitz, 38042 Grenoble Cedex 9, France*

[4]*European Spallation Source (ESS AB), St Algatan 4, Lund, Sweden*

[5]*School of Applied Science, University of Huddersfield, Huddersfield, HD1 3DH, United Kingdom*

[6]*RIKEN, 2-1 Hirosawa, Wako, Saitama 351-0198, Japan*

(Received 19 January 2012; revised manuscript received 29 March 2012; published 17 May 2012)

Longitudinal field (LF = 110 G) muon spin relaxation (μSR) has been used to investigate the pressure dependence ($P < 4.5$ kbar) of paramagnetic spin fluctuations in the spin glass alloy $Y(Mn_{0.95}Al_{0.05})_2$ via observation of the μ^+ spin depolarization. External mechanical force is seen to counteract the Al-induced chemical pressure, fully delocalizing the Mn moment and altering the nature of the spin fluctuation spectrum sensed by the muon. A qualitative change in the functional form of the μ^+ spin depolarization is observed. Complementary ambient and high-pressure neutron diffraction measurements suggest not only pressure-dependent structural transitions but also the instability of the localized manganese moment. The ambient and high-pressure μ^+ spin depolarization results from $Y(Mn_{0.95}Al_{0.05})_2$ are likened to $P = 0$ results reported for other $Y(Mn_{1-x}Al_x)_2$ alloys. Finally, the possibility of using μ^+ spin depolarization rates to predict experimental inelastic neutron scattering (INS) line widths is considered; the muon having the potential to provide information equivalent to that obtained via INS but with greatly reduced data collection times.

DOI: 10.1103/PhysRevB.85.184416 PACS number(s): 76.75.+i, 28.20.Cz, 75.50.Lk

I. INTRODUCTION

The cubic Laves phase compound YMn_2[1] is of interest since it allows theoretical advances that attempt to establish a unified understanding of magnetism to be evaluated.[2] A member of the RMn_2 (R = rare earth) family of alloys, YMn_2 is best described as a system of well-defined local moments below its antiferromagnetic (AF) ordering temperature ($T_N = 110$ K). In contrast, the paramagnetic phase is more accurately described using an itinerant electron picture within the framework of Moriya's self consistent renormalization (SCR) theory of spin fluctuations.

At room temperature, YMn_2 supports a cubic C15 structure with a lattice constant of 7.682 Å [3] ($V_{\text{unit cell}} = 453.34$ Å^3). Upon cooling, the lattice contracts until, at 110 K, a discontinuous, or first order, volume expansion of the unit cell is observed ($\Delta V/V = 5\%$). Correspondingly, the unit cell changes from a cubic (space group: Fd-3m) to tetragonal (space group: $F4_1/d\ 1\ 2/m$ ($I4_1/amd$)) geometry. Below 110 K, long-range antiferromagnetic (AF) order ensues with the system assuming a helically modulated magnetic structure with a periodicity of about 400 angstroms. Upon warming, marked hysteretic behavior is observed in both lattice parameter and magnetic susceptibility.[4] These uncommon magnetic properties are a result of i) the proximity of the system to Mn moment instability and ii) topological frustration arising from antiferromagnetic correlations on lattices of corner sharing tetrahedra.[5] The system exhibits large amplitude spin fluctuations[6] and a great sensitivity of the magnetic properties to the unit cell volume.

The first-order phase transition in YMn_2 is extremely sensitive to *mechanical* and *chemical* pressure. The Néel point may be fully suppressed by applying 2.7 kbar of external pressure or by inducing "chemical pressure" via, for example, the substitution of 2.5 at. % Fe for Mn.[7] Such results indicate that small reductions in the Mn-Mn nearest neighbor distance precipitate a collapse of AF order as the Mn moments revert to a spin-fluctuating state. It is worth mentioning that the existence of a threshold between localized and itinerant magnetism in RMn_2 intermetallic compounds was first observed using NMR.[8] In brief, Mn moment localization was purported to be governed by interatomic distance after the ^{55}Mn hyperfine field was seen to collapse for those RMn_2 alloys with cubic lattice constants less than approximately 7.52 Å (at 4.2 K).

In contrast, partial substitution of aluminium for manganese, i.e., $Y(Mn_{1-x}Al_x)_2$, is seen to expand the unit cell.[4] Here, the magnitude of the volume expansion at the Néel point decreases with increasing Al concentration until, for $Y(Mn_{0.90}Al_{0.10})_2$, no volume anomaly is observed. While the phase transition remains first order for $x < 0.03$, percolation of the Al atoms leads to a second-order progression for substituent concentrations greater than $x \sim 0.03$. Moreover, the Mn moments become progressively more localized with increasing Al content. Evidence for this itinerant-local moment crossover comes from the Curie-Weiss-like[4] appearance of high-temperature bulk susceptibility measurements as well as thermal expansion behavior in accordance with the predictions of SCR theory. Between $x \sim 0.03$ and $x \sim 0.10$, however, a highly frustrated magnetic ground state is observed. The evolution of diffuse magnetic Bragg peaks in neutron diffraction data,[9] in conjunction with field hysteresis in the susceptibility measurements, suggests short-range spin glass correlations in this compositional range.

Previously, to complement ongoing research into local and itinerant moment magnetism in RMn_2 alloys,[10,11] we used transverse field (TF) and zero-field (ZF) μSR to probe spin dynamics, the collapse of long range antiferromagnetic

order and the onset of magnetic frustration in $Y(Mn_{1-x}Al_x)_2$[12] ($0.0 < x < 0.30$). In C15 compounds, the muon is most likely to reside at the so-called (2-2) site,[13] with each muon having two Y atoms and two Mn atoms as nearest neighbors. As such, the muon proves itself to be a sensitive local probe of static and dynamic magnetic phenomena. For alloys with $x < 0.03$, we find that in the paramagnetic regime the μ^+ spin relaxation response exhibits characteristics analogous to that of a wholly spin fluctuating ground state. In contrast, muon spin relaxation observed from $Y(Mn_{0.90}Al_{0.10})_2$ favours the Kohlrausch form, as predicted for concentrated spin glass systems.[14] To further this work we have now used longitudinal field (LF = 110 Gauss) muon spin relaxation (μSR) to investigate the pressure dependence ($P < 4.5$ kbar) of paramagnetic spin fluctuations in the spin glass alloy $Y(Mn_{0.95}Al_{0.05})_2$ via observation of the μ^+ spin depolarization; an alloy which exhibits local moment Curie-Weiss-like characteristics but with an Al concentration bordering magnetic frustration.

Complementary neutron diffraction measurements, which illuminate crystallographic anomalies and pressure-dependent manganese moment stability, are also described. In addition, the ambient and high-pressure spin depolarization results from $Y(Mn_{0.95}Al_{0.05})_2$ are likened to μSR measurements (previously unpublished work or reported by other authors) from other $Y(Mn_{1-x}Al_x)_2$ alloys. Our results also add to previous neutron diffraction studies which report the influence of chemical pressure [$Y(Sc)(Mn_{1-x}Al_x)_2$][15] and applied external pressure [$Ho(Mn_{0.9}Al_{0.1})_2$][16] on other Al-doped Laves phase RMn_2 alloys.

A. Itinerant electron magnets and μ^+ relaxation: experimental SCR predictions

Qualitative SCR predictions for the temperature dependence of the muon response expected from different 'itinerant' systems in the paramagnetic regime are summarized below. While $Y(Mn_{1-x}Al_x)_2$ is not considered to be a weakly itinerant magnetic system, we report Moriya's findings here since we liken our ambient and high-pressure results to these predictions; application of pressure perhaps inducing a SCR response.

To summarize, the SCR[2] theory of spin fluctuations (i.e., electron-hole pair excitations) was developed by Moriya in 1985 from earlier self-consistent models by Moriya and Kawabata[17] and Murata and Doniach.[18] SCR was developed to address difficulties encountered using the Hartree-Fock random phase approximation (HF-RPA) method to describe the behavior of itinerant electron magnets. For example, SCR theory explains experimentally observed reduced ordered moment sizes, Curie-Weiss behavior of the uniform susceptibility and reduced transition temperatures. The ability to observe directly the $1/T_1$ relaxation of electron moments via the muon spin depolarization parameter λ ($=1/T_1$) using μSR allows the efficacy of SCR predictions to be tested. The evolution of the temperature dependence of $1/T_1$ expected from different 'itinerant' systems (for example, localized moment magnet (i.e., EuO) $\rightarrow$ itinerant ferromagnet (i.e., Fe) $\rightarrow$ weak itinerant ferromagnet (i.e., MnSi) $\rightarrow$ nonmagnetic metal (i.e., Al)) is given in Ref. 2. With regard to weakly ferromagnetic materials, SCR theory suggests that if the susceptibility, χ, follows the Curie-Weiss form, then the qualitative prediction for the temperature dependence of the muon spin depolarization above T_c is,

$$\lambda = \frac{1}{T_1} \propto \frac{T}{T - T_C} \tag{1}$$

In contrast, the temperature dependence of λ predicted using the HF-RPA[19] method is $1/T_1 \propto T/(T^2 - {T_C}^2)$, while a localized moment system usually does not depend upon temperature, except for a narrow critical region near the transition. Equation (1) has been successfully used to describe the temperature dependence of the measured spin-lattice relaxation rate in MnSi (Hayano *et al.*[20]); MnSi being an itinerant electron system that orders with a long period helical spin structure below a Curie temperature of $T_c \sim 30$ K. The muon measurements were taken with the sample subject to a longitudinal field of 122 Gauss to decouple the dynamical relaxation from the sizable static nuclear dipolar fields arising from ^{55}Mn nuclei. While the dynamic fluctuations of electron spins were too fast to observe at room temperature, closer to T_c measurable dynamical relaxation, well described using Eq. (1), became visible. More recently, μSR studies of weak itinerant electron ferromagnetism in Au_4V have also supported SCR predictions.[21] In contrast, for weak itinerant electron antiferromagnets,

$$\lambda = \frac{1}{T_1} \propto \frac{T}{(T - T_N)^{\frac{1}{2}}} \tag{2}$$

when the susceptibility displays Curie-Weiss behavior. Here, the muon spin depolarisation rate is predicted to increase with temperature as $\sqrt{T}$ for $T \gg T_N$. On the contrary, $\lambda(T)$ predicted using the HF-RPA method is $1/T_1 \propto T/(T^2 - T_N^2)^{1/2}$. To our knowledge, surprisingly few weak itinerant AF systems have been used to test Moriya's theory using muons. Perhaps the most widely studied itinerant electron system displaying strong antiferromagnetic spin fluctuations is YMn_2 itself.

II. EXPERIMENTAL DETAILS

Since μSR[13,22] and neutron diffraction[23,24] are well-established techniques, and described in detail elsewhere, only an overview pertinent to this work is given here.

A. Muon spin relaxation (μSR)

In ZF-μSR experiments, detectors are positioned along the muon beam direction in front of, and behind, the sample. Relaxation spectra are determined from the time-dependent positron count rates collected in the forward $F(t)$ and backward $B(t)$ detectors via the expression,

$$P_z(t) = A_o G_z(t) = \frac{F(t) - \alpha B(t)}{F(t) + \alpha B(t)} \tag{3}$$

where $P_z(t)$ describes the time dependence of the muon spin polarization. A_o is the initial asymmetry (i.e., the asymmetry at time $t = 0$) and α is a calibration term to account for the relative efficiencies of the counters in the forward and backward detectors and for absorption within the sample and sample environment apparatus. α is determined from

a spectrum collected with the sample subject to a small transverse magnetic field of 2 mT (20 Gauss). $G_z(t)$ is the longitudinal muon spin relaxation function.

In a system of concentrated static magnetic dipoles, the resulting internal magnetic field distributions in each of the x, y and z directions are Gaussian centered around zero. Larmor precession of muon spins in such an environment, averaged over all muon sites, leads to, a relaxation function of the form,[25]

$$G_z(t,\sigma) = \frac{1}{3} + \frac{2}{3}(1-\sigma^2 t^2)\exp\left(-\frac{\sigma^2 t^2}{2}\right) \quad (4)$$

where σ is the width of the Gaussian distribution. Equation (4) is known as the zero-field static Gaussian Kubo-Toyabe (K-T) relaxation function.[25] In contrast, rapid fluctuations of the internal magnetic fields, however, lead to motional narrowing and a simple exponential muon spin relaxation function is observed,

$$G_z(t) = \exp(-\lambda t) \quad (5)$$

where $\lambda = 2\sigma^2\tau_c$ and τ_c is the correlation time of field fluctuations. Fluctuation rates between 10^8 and 10^{13} Hz can be measured using μSR.

For concentrated spin glasses, numerical simulations of Ising systems by Ogielski[26] have shown that above the glass transition temperature, T_g, the local dynamic spin autocorrelation function is proportional to a stretched exponential, $\langle S_x(0)S_x(t)\rangle \propto q(t) \propto \exp(-(\lambda t)^{\beta'})$, with β' increasing from $1/3$ at the glass transition to unity at $4T_g$. A possible thermodynamic explanation of this behavior in spin glasses based upon the Tsallis concept of subextensive entropy in strongly interacting disordered systems has recently been proposed.[27] ZF-μSR studies by Campbell *et al.*[14] have demonstrated that longitudinal muon spin relaxation measurements are sensitive to such nonexponential, or Kohlrausch, spin relaxation in concentrated spin glass systems. Campbell shows that the corresponding muon relaxation function also takes the form,

$$P_z(t) \propto \exp[-(\lambda t)^{\beta}] \quad (6)$$

with $\lambda(T)$ diverging at the glass transition and $\beta(T)$ approaching $1/3$.

The high-pressure LF-μSR measurements presented here were collected using the RIKEN-RAL high-energy muon facility (Port 2) at the ISIS Pulsed Neutron and Muon source, Rutherford Appleton Laboratory, UK.[28,29] The powdered sample was loaded into a Copper-Beryllium (CuBe) pressure cell. Pressures within the cell were generated using a helium gas intensifier. The relative percentage of signal from the sample to signal from the CuBe cell was $\sim 20\%$; the physical thickness of the CuBe cell limiting sample volume. As a result, the high pressure measurements were performed in 110 G longitudinal field (LF) to greatly simplify the background response from the CuBe [Fig. 1]. The ambient pressure ($P =$ 0 kbar) LF-μSR (LF = 110 G) measurements presented here were collected using the MuSR facility at ISIS. The powdered sample was loaded into a flat plate silver sample holder. All muon relaxation spectra were analyzed using the WIMDA program suite.[30] For the high-pressure work ($P = 4.5$ kbar), the background response from the pressure cell was first fully characterized as a function of temperature and applied field. This background response was then adjusted, and fixed, temperature point by temperature point during the analysis of spectra collected from the sample. For both pressures ($P =$ 0 and $P = 4.5$ kbar), data was collected upon warming with the longitudinal field being applied after the sample had been cooled to base temperature in zero applied field.

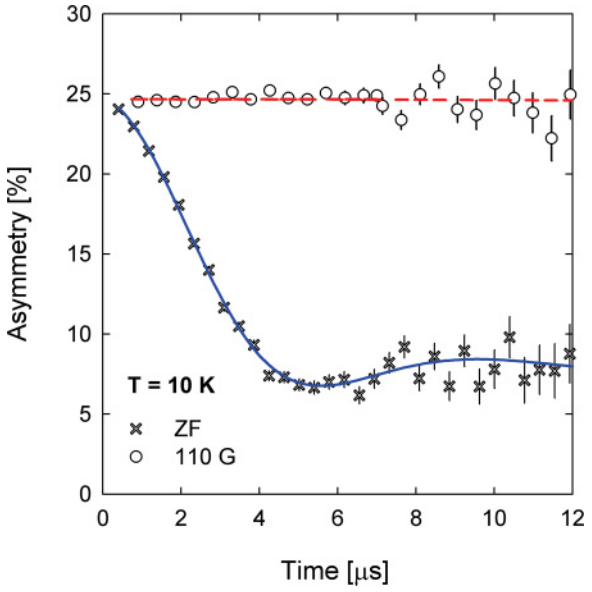

FIG. 1. (Color online) Suppression of nuclear dipole relaxation, associated with the CuBe pressure cell material, via application of an external longitudinal field of 110 G. The dashed line is the result of fitting the LF data (○) to a Gaussian relaxation function. The solid line is the result of fitting the ZF data (×) to a Kubo-Toyabe and a Gaussian relaxation function.

B. Nuclear Bragg diffraction

A couple of comments should be made regarding the analysis of neutron diffraction data. First, it is not the purpose of this work to refine the magnetic neutron scattering intensity but to simply observe and characterize its temperature dependence. A detailed study of the evolution of magnetic scattering from $Y(Mn_{1-x}Al_x)_2$ alloys at ambient pressure, as revealed using neutron spin polarization analysis, will be presented elsewhere. An overview of magnetic neutron diffraction can be found in the references given at the start of this section. Second, contamination of the $Y(Mn_{0.95}Al_{0.05})_2$ diffraction data at short d spacing by pressure-dependent Bragg reflections arising from solidified helium, as well as intense Bragg reflections from the Al pressure cell, precludes detailed structural analysis using the Rietveld method. Changes in the volume of the unit cell and/or structural anomalies are therefore gauged by either monitoring the d spacing associated with certain lattice reflections or via peak shape analysis of individual Bragg reflections. Such analysis was performed using the LeBail intensity extraction option coded into the profile refinement package, GSAS.[31]

High-pressure ($0 < P < 4.5$ kbar) neutron diffraction measurements were collected using the backscattering diffraction capabilities of the OSIRIS[32] instrument at ISIS. Previous

neutron work[3] shows the magnetic reflections from the helical magnetic structure assumed by YMn_2 below T_N to lie between approximately 2 and 5.5 Å. OSIRIS is ideally suited to probe such a d-spacing range and affords both high flux and resolution at the corresponding wavelengths (i.e., 4 – 10 Å). The sample was mounted in an aluminium pressure cell and high pressures were generated using a helium gas intensifier. Lattice spacings were determined using the profile refinement package GSAS.[31] Instrument-specific parameters necessary for the refinement procedure were determined by analyzing a neutron diffraction pattern collected from a National Institute of Standards and Technology (NIST) reference material; namely silicon (SRM640c).

C. Sample preparation

A 20 g polycrystalline ingot of $Y(Mn_{0.95}Al_{0.05})_2$ was prepared by melting together the appropriate quantities of 99.995% pure constituents using the argon arc melting technique. Losses were less than 2% and attributed to Mn evaporation during the melting process. To avoid formation of the highly magnetic impurity phase, Y_6Mn_{23}, excess Y was added to the level of 5%. The resulting ingot was sealed under vacuum in a quartz ampoule and annealed at 800 °C with subsequent quenching in liquid nitrogen. The alloy was crushed into a fine powder. The same $Y(Mn_{0.95}Al_{0.05})_2$ sample was used for both the neutron and muon work presented here.

III. RESULTS AND ANALYSIS

A. Neutron diffraction: Room temperature (290 K)

At room temperature, $Y(Mn_{0.95}Al_{0.05})_2$ exhibits the same cubic crystal structure (space group: Fd-3m) as the parent compound, YMn_2. The variation of the Fd-3m unit cell parameter at $T = 290$ K and as a function of (i) increasing external pressure (for the 5 at. % Al alloy) and (ii) increasing Al concentration is shown in Fig. 2. The data is compared to previously reported ambient pressure results.[33] No pressure-induced structural change is observed using OSIRIS. Instead, we find that at 290 K application of external pressure simply results in a linear decrease of the cubic cell parameter until, by 4.5 kbar, the lattice spacing of $Y(Mn_{0.95}Al_{0.05})_2$ resembles that of YMn_2.

B. Neutron diffraction: Base temperature (10 K)

Analysis of diffraction data collected from YMn_2 at 10 K, using OSIRIS, reveals that the parent compound favors a tetragonal, rather than cubic, unit cell at base temperature. A splitting of the (400) reflection into the (004) and (220) reflections is clearly observed, as shown in Fig. 3. This result is in excellent agreement with work reported by Cywinski *et al.*[3] using the high resolution diffractometer, HRPD (ISIS, $\Delta d/d \sim 10^{-4}$). The tetragonal space group [$F4_1/d\ 1\ 2/m\ (I4_1/amd)$] proposed by[3] for YMn_2 at 10 K was used to fit our OSIRIS data. We find that for YMn_2 in the tetragonal phase $a = b = 7.74$ Å, while $c = 7.702$ Å.

It is not unreasonable to suggest that $Y(Mn_{0.95}Al_{0.05})_2$ also undergoes a similar structural transformation. This hypothesis is supported by the weak structural anomaly observed in the temperature dependence of the (111) nuclear reflection at 100 K [see Fig. 6(c), top]. If correct, and also tetragonal in nature, then as Fig. 3 shows, the resolution of the OSIRIS instrument ($\Delta d/d \sim 10^{-3}$) is clearly not sufficient to resolve splitting of Bragg reflections arising from a tetragonal lattice. While LeBail peak shape analysis of the diffraction data using a tetragonal space group provides an adequate description, higher-resolution diffraction may elucidate subtle structural changes.

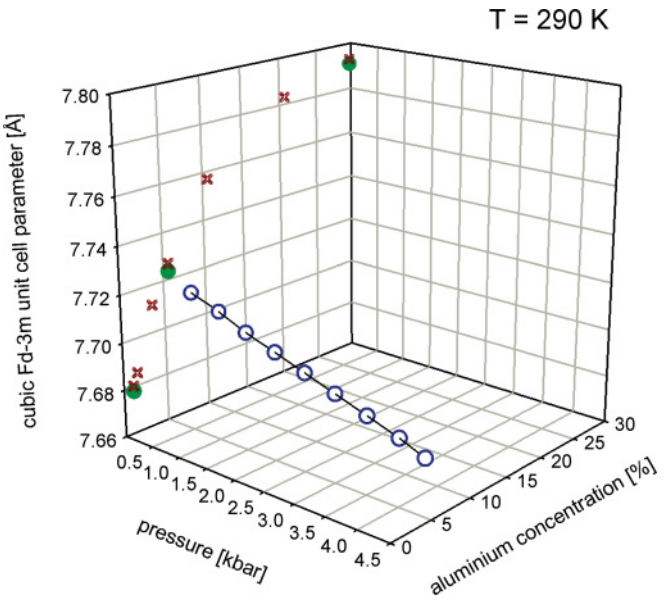

FIG. 2. (Color online) The variation of the cubic Fd-3m unit cell parameter at $T = 290$ K in $Y(Mn_{1-x}Al_x)_2$ as a function of (i) aluminum concentration (•) and, for 5 at. % Al, external pressure (○). The variation of cell parameter as a function of Al concentration as reported by Shiga *et al.*[34] is shown for reference (×).

It should also be noted that, unlike YMn_2, comparison of 10 and 250 K data reveals an increase in the intensity of all nuclear Bragg reflections at low temperature, by as much as $\Delta I_{10-250K}/I_{250K} = 14\%$ for the (111) reflection shown in Fig. 3. Such a response could suggest long-range ferromagnetic correlations. To test this hypothesis, we collected data from $Y(Mn_{0.95}Al_{0.05})_2$ at 10 K using the neutron polarization analysis technique (D7 diffuse scattering spectrometer, Institut Laue Langevin, Grenoble, France).[35] Our results show no evidence of magnetic scattering intensity at the nuclear Bragg positions (Fig. 4). Furthermore, we see no evidence of spin depolarization of the scattered neutron beam. Neutron spin depolarization would imply ferromagnetic correlations within the sample. We therefore attribute the origin of this increased scattering intensity at the nuclear positions to be structural rather than magnetic. It is also worth commenting that since D7 has very coarse instrumental resolution, and a limited Q range, any structural refinement of the nuclear scattering intensity would prove incomplete. A detailed overview of the neutron polarization analysis technique, the D7 spectrometer and complete analysis of magnetic scattering from our neutron diffraction and polarization studies of $Y(Mn_{0.95}Al_{0.05})_2$ will be presented elsewhere.

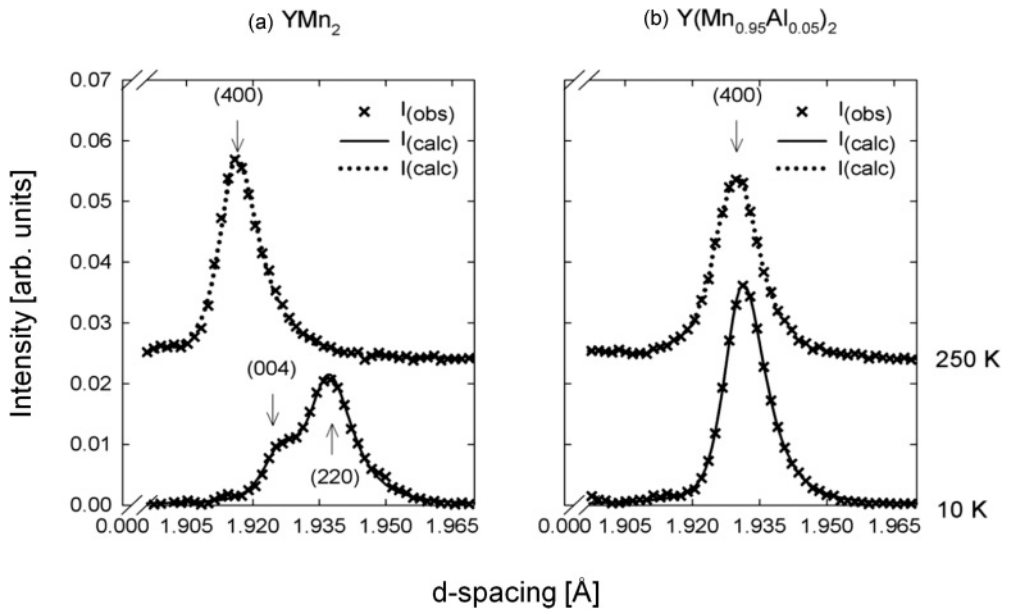

FIG. 3. (a) Tetragonal splitting of the YMn_2 (400) Bragg reflection at 10 K as observed using OSIRIS. The upper dashed line is a LeBail peak fit to 250 K data assuming cubic Fd-3m symmetry. The solid line is a LeBail peak fit to the 10 K data using the tetragonal ($I4_1$/amd) model. (b) Evolution of the (400) Bragg reflection for $Y(Mn_{0.95}Al_{0.05})_2$. The upper dashed line is a LeBail peak fit to 250 K data assuming cubic Fd-3m symmetry. While there is no visible splitting at 10 K, the solid line is a LeBail peak fit using the tetragonal ($I4_1$/amd) model. Peak analysis in this way suggest $a = b = 7.7115(5)$ Å and $c = 7.729(14)$ Å. The high-temperature data has been vertically offset for clarity.

Instead, weak antiferromagnetic satellite reflections are evident at base temperature and at d spacings of approximately 2.45, 3.14, 3.45, and 5.45 Å. These d spacings correspond to momentum transfer (Q) values of 2.56, 2.0, 1.82, and 1.15 $Å^{-1}$, respectively. Application of 4.5 kbar, however, is sufficient to completely suppress these magnetic reflections. As an example, the pressure dependence of the (2 0 1) antiferromagnetic Bragg reflection is presented in Fig. 5(b). The decrease in magnetic scattering intensity is accompanied by an anomalous decrease in the peak position of the nuclear (111) lattice reflection for pressures greater than 3.5 kbar, as illustrated in Fig. 5(a).

C. Neutron diffraction: Warming (10–250 K)

Upon warming, and with the $Y(Mn_{0.95}Al_{0.05})_2$ sample at ambient pressure, a structural anomaly is observed at approximately 100 K. The ambient pressure peak position of the (111) nuclear Bragg reflection is plotted as a function of temperature ($2 < T$ (K) < 250) in Fig. 6(c) [top]. In contrast, application of 4.5 kbar is sufficient to inhibit the volume expansion observed at 100 K when $P = 0$. Instead, we detect a weak structural anomaly closer to 50 K [Fig. 6(c), top].

As stated in the Introduction, Mn moment localization in RMn_2 alloys is reportedly governed by interatomic distance such that the Mn moment collapses for RMn_2 lattice constants less than approximately $d_c = 7.52$ Å at 4.2 K.[8] In the case of a cubic Laves phase alloy, this corresponds to a critical Mn-Mn distance of approximately 2.66 Å. For $Y(Mn_{0.95}Al_{0.05})_2$, however, collapse of long-range magnetic order below 4.5 kbar [Fig. 5(b)] does not appear to be a consequence of the unit cell parameter (d) crossing d_c. At room temperature we find that d falls linearly from 7.72 Å at ambient pressure to 7.68 Å by

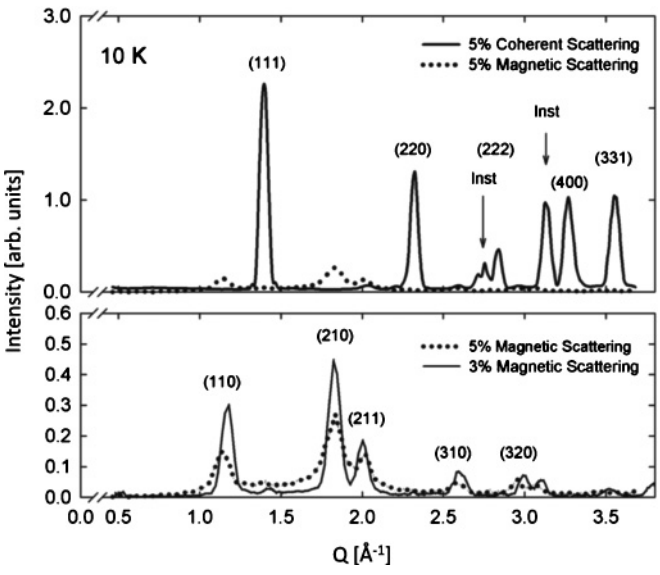

FIG. 4. Nuclear spin coherent (top) and magnetic scattering (bottom) from 5 at. % Al at 10 K. Magnetic scattering from 3 at. % Al is shown to accentuate the diffuse nature of the magnetic scattering from the 5 at. % Al alloy. The data was collected using the diffuse scattering spectrometer, D7, at the Institut Laue Langevin, Grenoble, France. Inst = Bragg reflections originating from the D7 instrument. The nuclear and magnetic peaks have been indexed according to Motoya.[9]

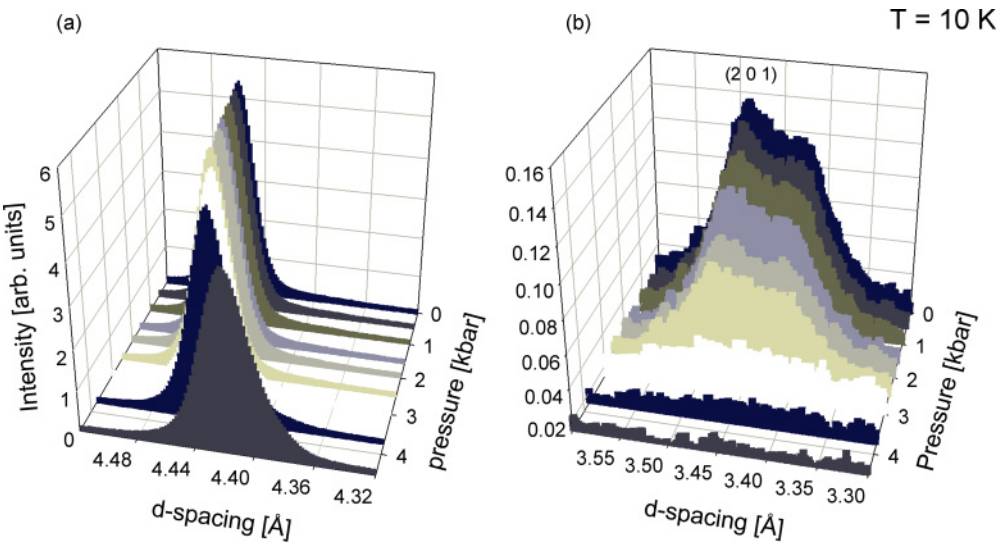

FIG. 5. (Color online) Pressure dependence of the (a) nuclear (111) and (b) antiferromagnetic (201) Bragg reflections at $T = 10$ K. The background from the empty pressure cell has been subtracted from the data.

$P = 4.5$ kbar (Fig. 2). Such a rate of compression corresponds to a bulk modulus, K_o (GPa) = volume * $\Delta P/\Delta V \sim 29$ GPa. This result is consistent with that reported for the parent compound, YMn_2.[36,37] For comparison, at 10 K (and assuming a cubic symmetry due to the limited instrument resolution) two distinct regions of compressibility are observed between ambient and the highest pressure. Below 3.5 kbar, a linear decrease in lattice parameter is observed with d reducing from 7.71 Å ($P = 0$) to 7.68 Å ($P = 3.5$). Such a change corresponds to a $\Delta V_{P=0-3.5}/V_{P=0} \sim 1\%$ and a bulk modulus value of 30 GPa. Above 3.5 kbar, however, an anomalous change in the rate of $d(P)$ is observed [see Fig. 5(a)]. While no meaningful bulk modulus information can be extracted for pressures greater than 3.5 kbar, this point of inflexion does correspond to the collapse of the local Mn moment. Nonetheless, applied external pressures less than 4.5 kbar (0.45 GPa) appear insufficient to drive d below the reported critical point; the cubic unit cell parameter of $Y(Mn_{0.95}Al_{0.05})_2$ at 4.5 kbar and 10 K being 7.64 Å. This may not be so surprising given that at ambient temperature approximately 3.5 GPa of pressure is required to drive the lattice parameter of YMn_2 from 7.68 to 7.52 Å.[36]

D. Longitudinal field Muon spin relaxation (LF-μSR)

Longitudinal field-μSR, in conjunction with the ARGUS CuBe high-pressure cell apparatus,[29] was used to investigate the collapse of magnetic order on a *local* level. As previously mentioned, both sample and empty pressure cell spectra were collected upon warming, and at the same temperatures, in a longitudinal field of 110 Gauss to greatly simplify the background response of the CuBe apparatus. We find no evidence to suggest that application of a longitudinal field of 110 G significantly perturbs the spin fluctuation spectrum of $Y(Mn_{0.95}Al_{0.05})_2$. We do observe slight recovery of μ^+ spin depolarization in 110 G compared to ZF. This result suggests a weak static contribution to the μ^+ depolarization measured in zero field. This static contribution most likely arises from nuclear dipoles. Application of 110 G is sufficient to suppress this static contribution, leaving only μ^+ depolarization originating from electronic fluctuations.

Depolarization spectra and associated fits to the data collected at ambient pressure and $P = 4.5$ kbar are shown in Figs. 6(a) and 6(b). The resulting fit parameters are compared in Figs. 6(c) and 6(d). We find that between 85 and 300 K, the ambient pressure data is well described by a stretched exponential relaxation function; full asymmetry (0.23) being recovered at short times at all temperatures within this regime. We find that β falls from unity at 280 K to 0.33 at 85 K as predicted for a concentrated spin glass system.[14] Correspondingly, the μ^+ spin depolarization rate (λ) starts to diverge below 120 K.

In contrast, a pressure of 4.5 kbar induces a simple, rather than *stretched,* exponential μ^+ spin relaxation response [Fig. 6(b)] between 50 and 280 K. The depolarization rate increases from 0.002 μs^{-1} at room temperature to 0.1 μs^{-1} at 50 K. The sudden drop in the asymmetry parameter (A_o) below 100 K indicates the presence of a *second* relaxing component. The rate of this relaxation process, however, is beyond the frequency resolution of the ARGUS instrument. As a result, we are unable to characterize the magnitude and temperature dependence of this additional relaxation term.

The temperature dependence of $\lambda(T, P = 0)$ and $\lambda(T, P = 4.5)$ is highlighted in Fig. 6(c). We find that over the temperature range studied $\lambda(T, P = 0)$ favors a critical scaling model, namely,

$$\lambda(T) = \lambda_o \left(\frac{T - T_{\text{trans}}}{T} \right)^{-\gamma} \tag{7}$$

which yields a transition temperature, T_{trans}, or in this case glass transition, $T_g = 88.2 +/- 0.2$ K with a critical exponent, γ, equal to $0.92 +/- 0.09$. A critical exponent of 0.92 is not unreasonable for a spin glass material. For example, previously reported values of γ range from 0.94 in the cluster glass CrFe (with 17 at. % Fe)[38] to 2.6 to 2.9 in the dilute spin glasses CuMn and AuFe.[39] Similar parameterization of the $P = 4.5$ kbar

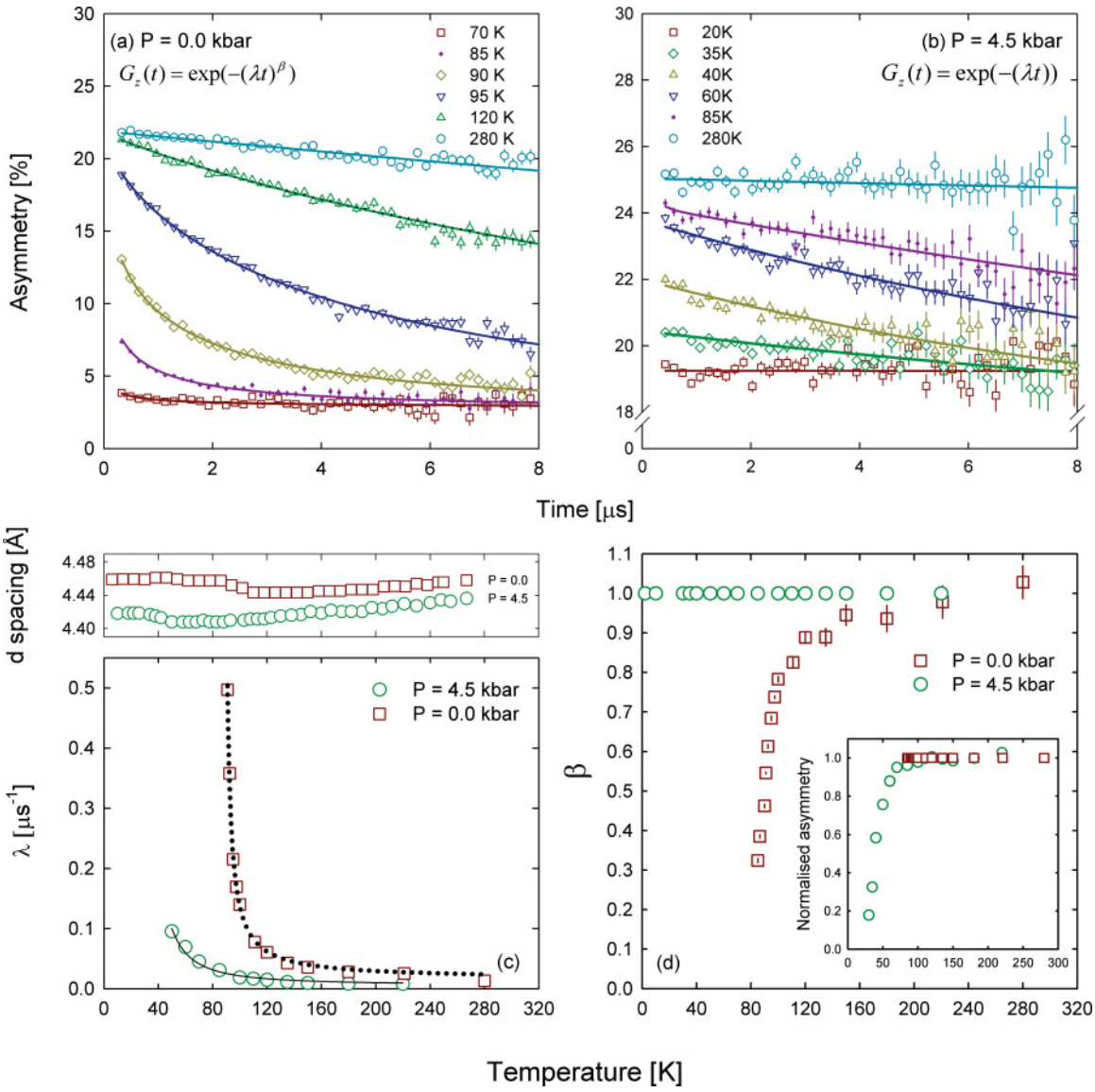

FIG. 6. (Color online) Muon spin relaxation spectra and associated fits to the data collected from $Y(Mn_{0.95}Al_{0.05})_2$ at (a) ambient pressure and (b) $P = 4.5$ kbar. Figure (b) highlights the sizable background signal (bck ~18%) originating from the CuBe pressure cell. (c) Comparison of μ^+ spin relaxation rates at ambient pressure and $P = 4.5$ kbar. The solid (Arrhenius fit) and dotted lines (critical form) are fits to the data as described in the text. Top: The temperature dependence of the peak position of the (111) nuclear Bragg reflection at 4.5 kbar and ambient pressure as revealed by neutron diffraction. The data suggests structural transitions at approximately 100 K ($P = 0$) and 50 K ($P = 4.5$). (d) Temperature and pressure dependence of the asymmetry (inset) and beta parameters used to model the observed muon spin depolarization. The asymmetry parameter has had the background component removed and been normalized to A_o(280 K).

data, however, is compromised by significant uncertainty in the resulting, and highly correlated, fit parameters. Instead, $\lambda(T, P = 4.5)$ is better described from 50 to 280 K using the Arrhenius form,

$$\lambda(T) = \lambda_o \exp\left(-\frac{E_a}{k_B T}\right) \tag{8}$$

with $E_a/k_B = 150 +/- 9$ K. The changing nature of the temperature dependence of $\lambda(T,P)$ is accentuated in Fig. 7(b), where our μ^+ spin depolarization results from $Y(Mn_{0.95}Al_{0.05})_2$ are compared to published, and previously unreported, ambient-pressure relaxation rates from other $Y(Mn_{1-x}Al_x)_2$ alloys; namely (i) the parent compound, YMn_2[3] (TF measurement, MuSR spectrometer), (ii) an alloy with 10 at. % Al[12] (ZF measurement, MuSR) and (iii) $Y(Mn_{0.70}Al_{0.30})_2$ (ZF, MuSR, previously unpublished). The data points shown have been extracted from the references given. Like $Y(Mn_{0.95}Al_{0.05})_2$ at $P = 0$, the temperature dependence of μ^+ spin relaxation from YMn_2 is well described using Eq. (7). Modeling the data in this manner gives a Néel temperature of 93 +/− 7 K. T_N determined in this way is in good agreement with previously reported values.[4] In contrast, while adequately described using Eq. (7),[12] the temperature dependence of $\lambda(T)$ from $Y(Mn_{0.90}Al_{0.10})_2$, as

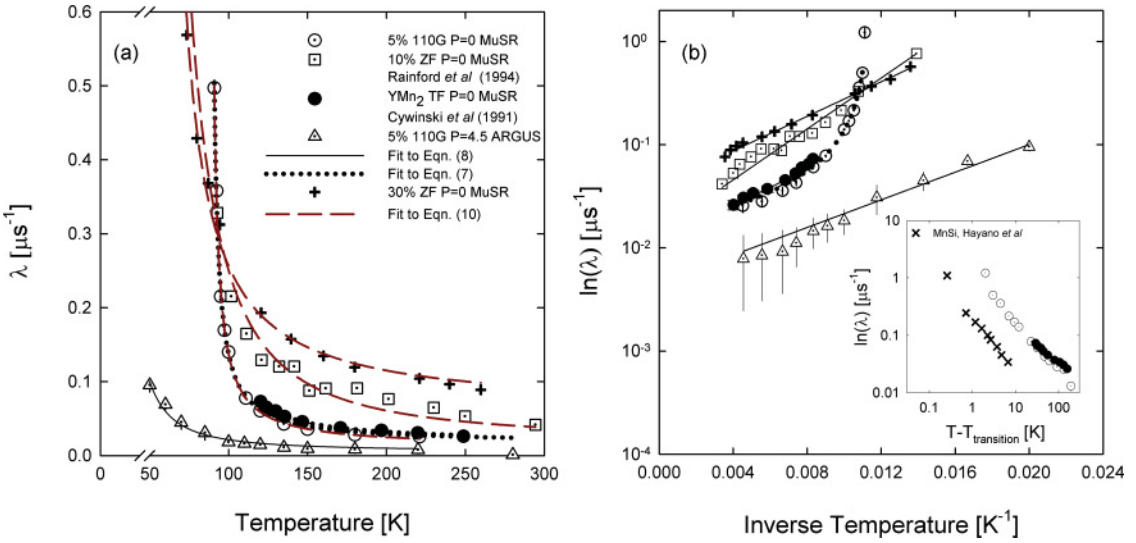

FIG. 7. (Color online) (a) Comparison of μ^+ spin depolarization rates collected from $Y(Mn_{0.95}Al_{0.05})_2$ [$P = 0.0$ (⊙) and 4.5 kbar (△)] with other reported, and previously unpublished, $Y(Mn_{1-x}Al_x)_2$ ambient pressure data; namely, YMn_2[3] (•, TF measurement), $Y(Mn_{0.90}Al_{0.10})_2$[12] (⊡, ZF), and $Y(Mn_{0.70}Al_{0.30})_2$ (+, ZF, unpublished). The lines are fits to the data as described in the text. (b) μ^+ spin depolarization rates plotted as ln(λ) vs. T^{-1} to accentuate the changing temperature, pressure, and concentration dependence of $\lambda(T,P)$. The solid or dotted lines are fits to the data as described in the text. Inset: the magnitude of μ^+ spin depolarization rates from YMn_2 and $Y(Mn_{0.95}Al_{0.05})_2$ compared directly to the response reported for the weak itinerant electron ferromagnet, MnSi, as presented by Hayano in.[20]

well as $Y(Mn_{0.70}Al_{0.30})_2$, is best described using the Arrhenius form, as illustrated in Fig. 7(b).

IV. DISCUSSION

We have used complimentary longitudinal field (LF = 110 Gauss) muon spectroscopy (μSR) and neutron diffraction techniques to probe the pressure dependence of magnetic order in $Y(Mn_{0.95}Al_{0.05})_2$ on a *bulk* (structure, neutron) and *local* (dynamical, muon) level. The muon spin relaxation results are compared to those reported for other $Y(Mn_{1-x}Al_x)_2$ alloys at ambient pressure.

For $Y(Mn_{0.95}Al_{0.05})_2$, ambient-pressure muon spectra are well described at all temperatures in the paramagnetic regime ($T > 100$ K) using a muon spin depolarization function of stretched exponential form. On a local scale at least, this response is indicative of a broadening distribution of relaxation rates, as witnessed by the tendency of β to fall to approximately 1/3 by 85 K and an accompanying divergence of the μ^+ depolarization rate below approximately 110 K. Over this temperature range (85 K $< T <$ 110 K) neutron diffraction measurements suggest that the alloy undergoes a weak structural distortion; a distortion accompanied by the onset of antiferromagnetic (AF) satellite reflections. Considering the diffuse nature of the magnetic structure, and the weak accompanying volume anomaly that signifies the localization of the Mn moments, it is likely that such a distribution arises from regions of well-localized, interacting, but topologically exchange frustrated Mn spins which, at low temperatures, form a concentrated spin glass-like phase. The temperature dependence of $\lambda(T,P = 0)$ is well described using a critical scaling model with a scaling exponent equal to unity. It is interesting to note that modeling $\lambda(T,P = 0)$ from $Y(Mn_{0.95}Al_{0.05})_2$, and YMn_2, using the critical form gives, within error, a value for γ equal to unity. For $\gamma = 1$, Eq. (7) reduces to Eq. (1); the SCR prediction for a weak itinerant electron ferromagnet. This result is perhaps not so surprising considering the Curie-Weiss temperature dependence of the local susceptibility displayed by these two alloys.[40] While we have no reason to describe these materials as weak itinerant electron ferromagnetic systems, the magnitude of the μ^+ spin depolarization rate determined from YMn_2 and $Y(Mn_{0.95}Al_{0.05})_2$ ($P = 0$) is likened [Fig. 7(b), inset] to the response reported for a weak itinerant electron ferromagnet, namely MnSi,[20] for comparison.

Application of 4.5 kbar external pressure, however, induces a substantial change in both the observed form of the muon spin depolarization function and the temperature dependence of $\lambda(T)$. Rather than stretched behavior, $G_z(T,$ 4.5 kbar) is seen to favor a simple exponential form. Such a response suggests that the muon senses a single spin depolarization rate, which is uncharacteristic of a wholly frustrated ground state. Indeed, under 4.5 kbar of applied external pressure, the spin depolarization rate is considerably less than that observed at $P = 0$. For example, at 150 K the ambient pressure relaxation rate is $\lambda(T,P = 0) = 0.0393 +/- 0.002\ \mu s^{-1}$, whereas under 4.5 kbar of applied pressure the system exhibits a depolarization rate of $\lambda(T,P = 4.5) = 0.0169 +/- 0.0026\ \mu s^{-1}$. This result indicates that the application of 4.5 kbar induces *either* substantially smaller internal fields or faster spin fluctuations. In contrast to the ambient pressure response, not only do paramagnetic spin fluctuations appear to exist down to approximately 50 K but the divergence of $\lambda(T,P =$ 4.5) suggests that the muon senses a magnetically driven transition at this lower temperature. Further evidence for a transition is signified by the response of the initial asymmetry parameter, $A_o(T,$4.5 kbar). The temperature dependence of A_o suggests that this transition is not only discontinuous but that

a second rapid depolarization process, beyond the frequency window of the ARGUS spectrometer, is present. The presence of this additional, yet immeasurable, relaxation process at short times suggests that *below* 100 K, application of 4.5 kbar induces large, initially inhomogeneous, internal fields at the μ^+ site which rapidly depolarize all nearby muons. Indeed, the pressure-induced change in the nature of the spin fluctuation spectrum is further illuminated by the evolution of the temperature dependence of $\lambda(T,P)$; from following a critical scaling model at $P = 0$ to an Arrhenius response by $P = 4.5$.

The changes observed in the muon response at 4.5 kbar can be related to structural changes observed on a bulk level using neutron diffraction. First, it is worth mentioning that at room temperature ($T = 290$ K) application of external pressure results in a linear decrease of the cubic unit cell parameter until, by 4.5 kbar, the volume of the unit cell of $Y(Mn_{0.95}Al_{0.05})_2$ is comparable to that of the parent compound, YMn_2. Nonetheless, despite exhibiting a unit cell comparable to that of YMn_2, application of 4.5 kbar does not induce the same spin depolarization rate. Second, neutron diffraction data collected at 10 K shows that application of 4.5 kbar is sufficient to completely inhibit formation of the antiferromagnetic satellite reflections observed at ambient pressure; hence localization of the Mn moments. The pressure dependence of the (201) AF reflection at 10 K suggests that the collapse of the Mn moment begins at approximately 2.5 kbar. Furthermore, the onset of this collapse seems coincident with the structural anomaly seen in the pressure-dependent peak position of the (111) nuclear Bragg reflection. It is likely that the observed reduction in lattice spacing is driven by a magneto-volume effect related to the collapse of the local Mn moments; local moments which, as seen in YMn_2, serve to expand the unit cell. It is not unreasonable to suggest, therefore, that when subject to an external pressure of $P = 4.5$ kbar, the Mn moment becomes inherently unstable and the system reverts to a wholly itinerant, rather than local moment, state. Maintaining 4.5 kbar, and warming the sample from base temperature to room temperature, results in a weak structural anomaly at ~50 K. It is interesting to note that the divergence of the muon spin depolarisation rate, $\lambda(T,P = 4.5)$, is coincident with this structural change. It is likely that the structural change is linked to the magnetic phenomena driving the muon response. On a bulk level, however, no long-range magnetic order is observed in the neutron diffraction data available. It is, of course, possible that the upper working pressure (5.0 kbar) of the CuBe cell is insufficient to fully transform the sample; as suggested by the continuously evolving position of the (111) nuclear reflection in Fig. 5(a). Nonetheless, as we have shown in $Cr_{1-x}Mo_x$,[41] the muon is supremely sensitive to weak magnetic phenomena. At this stage, the mechanism driving this structural anomaly, and hence the nature of the transition, is not clear. Nonetheless, considering the qualitative SCR predictions given previously, our results suggest that application of 4.5 kbar does not induce a response in $\lambda(T,P = 4.5)$ indicative of a weak itinerant ferromagnetic or antiferromagnetic ground state.

Muon spin depolarization rates from four $Y(Mn_{1-x}Al_x)_2$ alloys ($\leqslant$30 at. % Al) at ambient pressure are compared in Fig. 7. The magnitude of the transverse field muon spin depolarization rate reported for YMn_2 in the paramagnetic phase ($T > 110$ K) is comparable to that measured from $Y(Mn_{0.95}Al_{0.05})_2$; despite $G_z(t)$ for YMn_2 favoring a simple, rather than stretched, exponential form. In contrast, the magnitude of $\lambda(T)$ for alloys with 5 at. % Al $< x \leqslant 30$ at. % Al shows a marked increase with increasing Al substitution. Like $Y(Mn_{0.95}Al_{0.05})_2$, $G_z(t)$ for the 10 at. % Al and 30 at. % Al alloys assumes the stretched form.[12] However, the threefold increase in spin depolarization rate observed from the 10 at. % Al alloy (and which is further accentuated by 30 at. % Al) is likely to arise from larger fields or slower spin fluctuations at the muon site. Of the two scenarios, the latter is deemed more likely considering previously reported inelastic neutron scattering line width, $\Gamma(T)$, studies of spin fluctuations in $Y(Mn_{1-x}Al_x)_2$ alloys.[40] Such a result is perhaps unsurprising considering the ever more localized nature of the Mn moment with increased Al doping.

Finally, it is worth concluding by commenting that our ambient pressure results from $Y(Mn_{0.95}Al_{0.05})_2$ further support predictions that the temperature dependence of $\lambda(T, P = 0)$, as determined from the muon on a local level, may be directly compared with bulk inelastic neutron scattering line-width measurements, $\Gamma(T)$, via the formalism described by Lovesey.[42] To summarize,[12] the depolarization rate, $\lambda(T)$, may be related to the neutron line width, $\Gamma(Q)$, using the expression,

$$\lambda(T) = \frac{BT\chi_L}{\Gamma(Q)} \tag{9}$$

Preceding inelastic neutron scattering measurements[9,43] reveal that in $Y(Mn_{0.9}Mn_{0.1})_2$ not only is the inelastic line width relatively independent of wave vector, Q, but varies with temperature according to the Arrhenius law, i.e., $\Gamma(T) = \Gamma_o \exp(-E_a/k_BT)$. Moreover, the local susceptibility in this alloy is seen to be Curie-Weiss like, i.e., $\chi_L(T) = C/(T + \theta_w)$. Consequently, the expression for $\lambda(T)$ can be written,

$$\lambda(T) = \frac{cT}{(T+\theta_w)\exp(-E_a/k_BT)} \tag{10}$$

where $c = BC/\Gamma_o$. Here, the activation energy (E_a) and Curie-Weiss (θ_w) temperature parameters are derived from neutron scattering line width analysis. This model assumes (i) that the inelastic line width is relatively insensitive to momentum transfer, (ii) the inelastic line width varies with temperature according to the Arrhenius form and (iii) the T dependence of the local susceptibility, χ_L, of the Mn atoms is Curie-Weiss like. While inelastic neutron scattering has validated these assumptions for 3 at. % Al and 10 at. % Al alloys, they are yet to be tested from a neutron perspective for a 5 at. % Al sample. Nonetheless, it is not unreasonable to hypothesize that these assumptions also hold for alloys in the intermediate compositional range, i.e., 3 at. % Al $< x <$ 10 at. % Al. While Eq. (10) does provide a remarkably accurate description of the ambient pressure 5 at. % Al data (fit parameters: $E_a/k_B = 35$ K and $\theta_w = -88$ K), it should be noted that the fit shown in Fig. 7(a) is relatively insensitive to θ_w. Nonetheless, a negative value of θ_w is consistent with the predominately antiferromagnetic exchange interactions expected from this system. Further measurements, using both other $Y(Mn_{1-x}Mn_x)_2$ alloys and other magnetic systems, are necessary to test the full efficacy of Eq. (10) once experimentally determined E_a/k_B and θ_w

parameters derived from inelastic neutron measurements are incorporated. It is worth mentioning, however, that $\lambda(T,P = 0)$ from $Y(Mn_{0.70}Al_{0.30})_2$ is also well described using Eq. (10); the fit suggesting a negative Curie temperature [Fig. 7(a)].

V. SUMMARY

We have used longitudinal field (LF = 110 G) muon spin relaxation (μSR) to investigate the pressure dependence ($P < 4.5$ kbar) of paramagnetic spin fluctuations in the spin glass alloy $Y(Mn_{0.95}Al_{0.05})_2$ via observation of the μ^+ spin depolarization. Compared to ambient pressure measurements, external mechanical force is seen to counteract the Al-induced chemical pressure and significantly alter the nature of the spin fluctuation spectrum sensed by the muon. Complementary high-pressure neutron diffraction measurements show that application of 4.5 kbar is sufficient to fully delocalize the Mn moment and induce a wholly spin fluctuating magnetic ground state. Such high pressure also precipitates a weak structural transition at 50 K coincident with a divergence in the μ^+ spin depolarization rate. Such a response is indicative of a magnetic transition. While the mechanism driving this structural anomaly is unclear, the temperature dependence of $\lambda(T,P = 4.5)$ is not suggestive of a weak itinerant ferromagnetic or antiferromagnetic ground state as predicted by SCR theory.

The ambient and high pressure μ^+ spin depolarization results from $Y(Mn_{0.95}Al_{0.05})_2$ are also likened to ambient pressure results reported for other $Y(Mn_{1-x}Al_x)_2$ alloys. A distinct change in the magnitude and temperature dependence of the muon depolarization rate is observed with increasing Al substitution; from critical scaling ($x < 5$ at. % Al) to Arrhenius behavior (5 at. % Al $< x \leqslant 30$ at. % Al). The efficacy of describing μ^+ spin-depolarization data using theory developed to predict inelastic neutron scattering line widths has been further tested and found to provide a realistic description of the muon data. Future effort will test the applicability of the model once experimentally determined parameters from neutron measurements are incorporated. Nonetheless, the results presented here give further weight to complementarities between neutron and muon techniques. The muon has the potential to provide information that is largely equivalent to that obtained from inelastic neutron scattering measurements (at least for systems in which a relatively Q-independent line width is observed) but with greatly reduced sample masses and data collection times.

ACKNOWLEDGMENTS

The authors thank the United Kingdom's Science and Technology Facility Council for access to the ISIS facility, Rutherford Appleton Laboratory. The authors also thank Adrian Hillier, Peter Baker, and Steve Cottrell for their help and suggestions during the experiment. K.J.E. acknowledges EPSRC for financial support through the award of a "Next Generation Facilities User" postgraduate studentship.

*mark.telling@stfc.ac.uk

[1] F. Laves, Naturwissenshaften **27**, 65 (1939).
[2] T. Moriya, *Spin Fluctuations in Itinerant Electron Magnetism* (Springer-Verlag, Berlin, 1985).
[3] R. Cywinski, S. H. Kilcoyne, and C. A. Scott, J. Phys.: Condens. Matter **3**, 6473 (1991).
[4] M. Shiga *et al.*, J. Phys. F **17**, 1781 (1987).
[5] J. N. Reimers, A. J. Berlinsky, and A. C. Shi, Phys. Rev. B **43**, 865 (1991).
[6] B. D. Rainford, in *Muon Science: Muons in Physics, Chemistry and Materials*, edited by S. L. Lee, S. H. Kilcoyne, and R. Cywinski (IOP Publishing, Bristol, 1999).
[7] R. Cywinski *et al.*, Hyperfine Interact. **64**, 427 (1990).
[8] K. Yoshimura, M. Shiga, and Y. Nakamura, J. Phys. Soc. Jpn. **55**, 3585 (1986).
[9] K. Motoya, J. Phys. Soc. Jpn. **55**, 3733 (1986).
[10] M. T. F. Telling, C. Ritter, and R. Cywinski, J. Magn. Magn. Mater. **177**, 1480 (1998).
[11] M. T. F. Telling, C. Ritter, and R. Cywinski, Physica B **276**, 740 (2000).
[12] R. Cywinski and B. D. Rainford, Hyperfine Interact. **85**, 215 (1994).
[13] A. Schenck, *Muon Spin Rotation Spectroscopy* (Adam Hilger, Bristol, 1985).
[14] I. A. Campbell *et al.*, Phys. Rev. Lett. **72**, 1291 (1994).
[15] H. Nakamura *et al.*, J. Phys. Soc. Jpn. **65**, 2779 (1996).
[16] I. Mirebeau, I. N. Goncharenko, and I. V. Golosovsky, Phys. Rev. B **64**, 140401(R) (2001).
[17] T. Moriya and A. Kawabata, J. Phys. Soc. Jpn. **35**, 669 (1973).
[18] K. K. Murata and S. Doniach, Phys. Rev. Lett. **29**, 285 (1972).
[19] T. Moriya and K. Ueda, Solid State Commun. **15**, 169 (1974).
[20] R. S. Hayano *et al.*, Phys. Rev. Lett. **41**, 1743 (1978).
[21] K. Ellis *et al.*, Physics Procedia (in press, 2012).
[22] A. Yaouanc and P. Dalmas de Reotier, *Muon Spin Rotation, Relaxation, and Resonance: Applications to Condensed Matter* (Oxford University Press, New York, 2011).
[23] G. E. Bacon, *Neutron Diffraction* (Clarendon Press, Oxford, 1975).
[24] C. G. Windsor, *Pulsed Neutron Scattering* (Taylor and Francis, New York, 1981).
[25] R. Kubo and T. Toyabe, *Magnetic Resonance and Relaxation* (North Holland, Amsterdam, 1967).
[26] A. T. Ogielski and I. Morgenstern, Phys. Rev. Lett. **54**, 928 (1985).
[27] R. M. Pickup *et al.*, Phys. Rev. Lett. **102**, 097202 (2009).
[28] T. Matsuzaki, K. Ishida, K. Nagamine, I. Watanabe, G. H. Eaton, and W. G. Williams, The RIKEN-RAL pulsed Muon Facility, Nucl. Instrum. Meth. Phys. Res. A 465, 365 (2001).
[29] I. Watanabe *et al.*, Physica B: Condensed Matter **404**, 993 (2009).
[30] F. L. Pratt, Physica B **289-290**, 710 (2000).
[31] A. C. Larson and R. B. Von Dreele, *General Structure Analysis System (GSAS)*, Los Alamos National Laboratory Report LAUR 86-748 (2004).
[32] M. T. F. Telling and K. H. Andersen, Phys. Chem. Chem. Phys. **7**, 1255 (2005).
[33] M. Shiga, Physica B&C **149**, 293 (1988).
[34] M. Shiga *et al.*, J. Phys. Soc. Jpn. **57**, 3141 (1988).

[35]J. R. Stewart *et al*., J. Appl. Crystallogr. **42**, 69 (2009).
[36]A. Lindbaum *et al*., J. Phys.: Condens. Matter **11**, 1189 (1999).
[37]H. Sugiura *et al*., J. Alloys Compd. **367**, 230 (2004).
[38]M. T. F. Telling and R. Cywinski, J. Magn. Magn. Mater. **140**, 45 (1995).
[39]Y. J. Uemura *et al*., Phys. Rev. B **31**, 546 (1985).
[40]B. D. Rainford, R. Cywinski, and S. J. Dakin, J. Magn. Magn. Mater. **140**, 805 (1995).
[41]M. T. F. Telling, S. H. Kilcoyne, and R. Cywinski, Hyperfine Interact. **85**, 209 (1994).
[42]S. W. Lovesey, A. Cuccoli, and V. Tognetti, Hyperfine Interact. **64**, 321 (1990).
[43]K. Motoya *et al*., Phys. Rev. B **44**, 183 (1991).